Supplementary Material for: *Future extratropical cyclones with more moisture and fewer associated atmospheric rivers*

Patricia Coll-Hidalgo[1], Luis Gimeno-Sotelo[2,3], José C. Fernández-Alvarez[1,4,5], Raquel Nieto[1,4] and Luis Gimeno*[1,4]

[1] Environmental Physics Laboratory (EPhysLab), Centro de Investigación Mariña, Universidade de Vigo, Campus As Lagoas s/n, 32004 Ourense, Spain.

[2] Departamento de Ciências Matemáticas, Faculdade de Ciências, Universidade de Lisboa, Lisboa, Portugal.

[3] CEAUL - Centro de Estatística e Aplicações, Faculdade de Ciências, Universidade de Lisboa, Lisboa, Portugal.

[4] Galicia Supercomputing Center (CESGA), Climate System Research Unit, Santiago de Compostela, 15705, Spain.

[5] CESAM, Departamento de Física, Universidade de Aveiro, 3810-193, Aveiro, Portugal.

***Corresponding author:** Luis Gimeno (`l.gimeno@uvigo.es`)

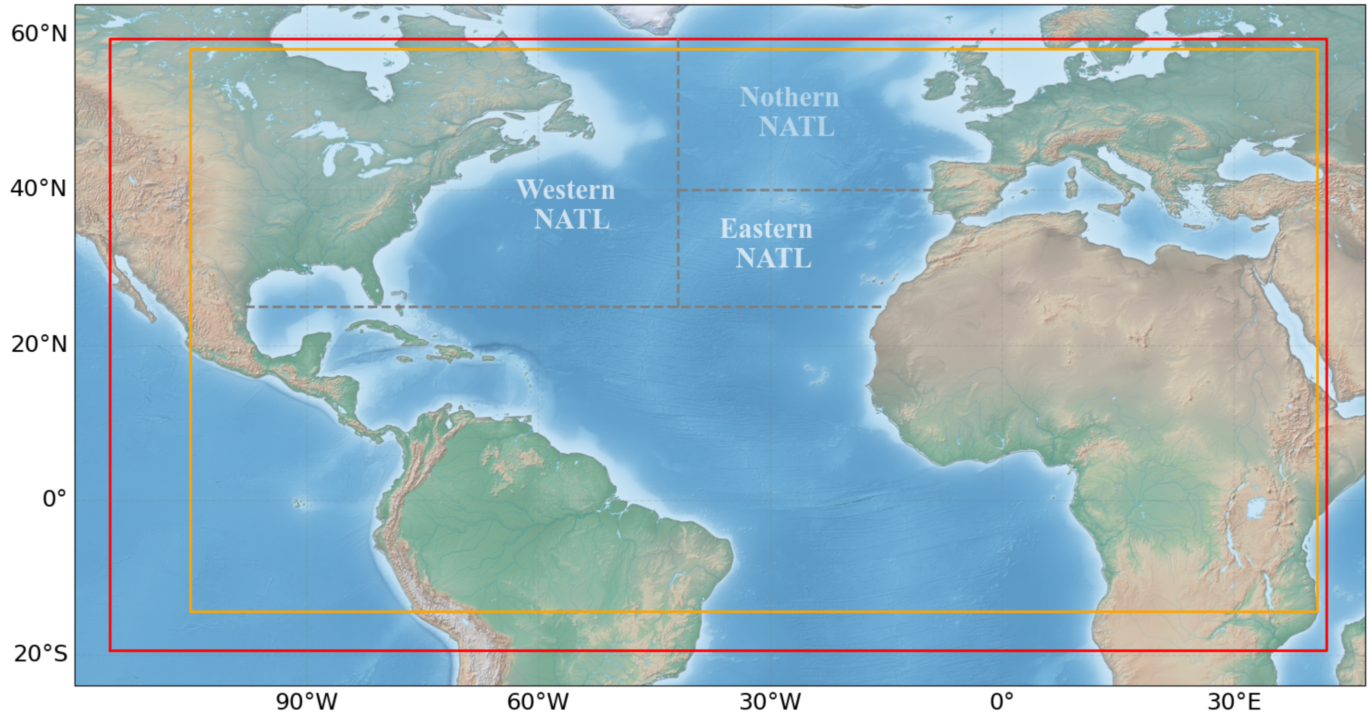

Figure S1 | Simulation domains used in this study. The WRF model dynamically downscaled the CESM2 outputs under the high-emission SSP5-8.5 scenario at ∼0.18° resolution over the outer red box domain (115.39°W–42.02°E, 19.41°S–59.51°N). The inner yellow box marks the FLEXPART simulation domain. Labelled North Atlantic (NATL) subregions: western NATL, eastern NATL, and northern NATL.

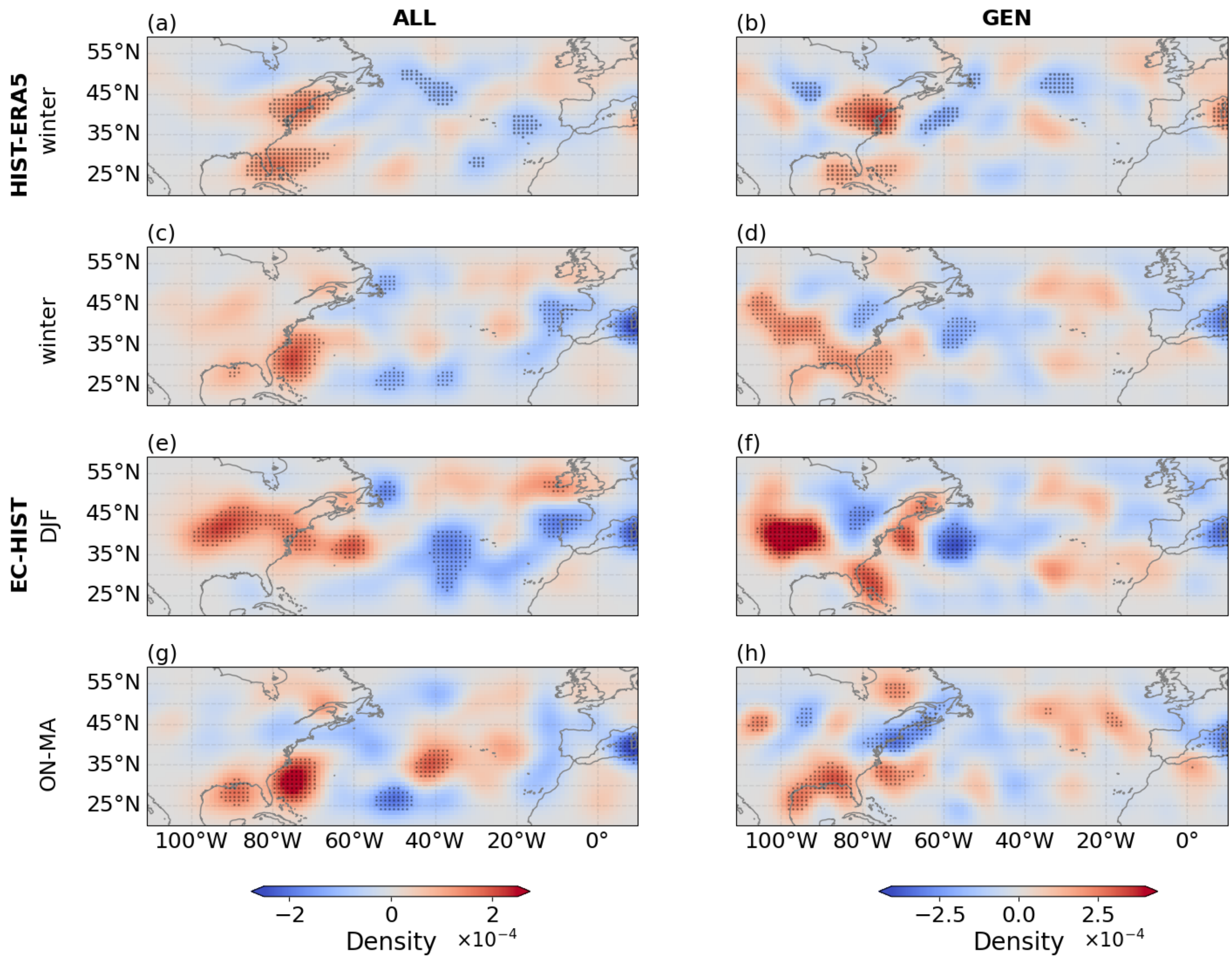

Figure S2 | Extratropical cyclone track and genesis density differences over the North Atlantic (1° × 1° grid). Climatological extratropical cyclone (ETC) track density differences between the ERA5 reanalysis and downscaled CESM2 historical simulations (HIST) during the extended winter (November–April 1985–2014). (b) Same as (a) but for the ETC genesis density. (c–h) Differences in ETC track (left) and genesis (right) densities between end-of-century (EC; 2070–2100) and HIST CESM2 simulations for (c, d) extended winter (November–April), (e, f) peak winter (December–February), and (g, h) transitional months (October, November, March, April). Statistically significant anomalies (standard deviation > 2) are marked with black dots.

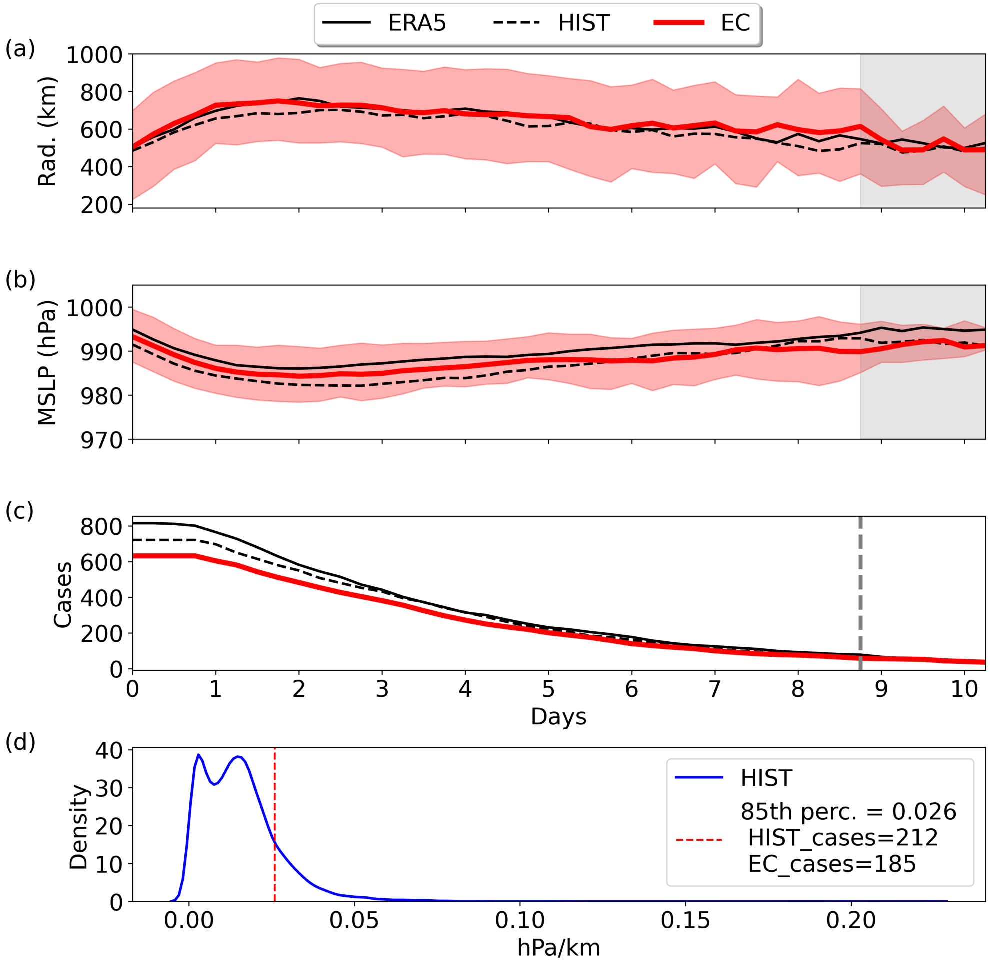

Figure S3 | Evolution of North Atlantic extratropical cyclone characteristics in the ERA5 and downscaled CESM2 datasets. Mean central sea level pressure (a) and cyclone radius (b) averaged over the 10-day lifecycle of extratropical cyclones tracked during the extended winter over the North Atlantic (NATL). Data are shown for the ERA5 reanalysis (1985–2014), CESM2 historical simulations (HIST, 1985–2014), and CESM2 end-of-century projections (EC, 2070–2100). (c) Number of cyclone cases contributing to six-hour estimates. The dashed vertical line in (c) indicates where case counts fall below 30% of the peak sample size for all datasets. The corresponding shaded regions in (a, b) mark intervals with reduced sample sizes (<30%). The shaded bands for EC in (a, b) represent the interquartile range (25th–75th percentile), indicating variability. (d) Density distribution of the radial pressure gradient, defined as the difference between the central mean sea level pressure and the mean sea level pressure at the outermost closed isobar, for the ETCs tracked in the HIST dataset. The 85th percentile of the distribution is indicated by the red dashed line.

Quantile permutation test results comparing future and historical extratropical cyclones (ETCs) across different cyclone association types fully, highly, moderately, and weakly associated. One-tailed p values < 0.05 are shaded.

Table S1 | Central mean sea level pressure (MSLP, hPa) of the ETCs.

Group	Quantile	Obs. Diff.	p-value
Fully	0.25	2.0968	1.40E-01
	0.50	4.2265	4.90E-02
	0.75	5.5165	4.80E-03
High	0.25	0.5955	4.46E-01
	0.50	-0.0800	4.67E-01
	0.75	0.6090	4.31E-01
Medium	0.25	6.7860	7.05E-02
	0.50	1.9150	3.85E-01
	0.75	1.1115	2.70E-01
Low	0.25	-7.5630	2.94E-01
	0.50	-4.1785	2.77E-01
	0.75	1.2380	3.90E-01

Table S2 | ETC radius (km).

Group	Quantile	Obs. Diff.	p-value
Fully	0.25	17.3224	2.45E-01
	0.50	11.4898	3.70E-01
	0.75	49.9686	9.60E-02
High	0.25	-8.3657	4.11E-01
	0.50	21.2115	2.83E-01
	0.75	38.8093	2.57E-01
Medium	0.25	-24.1853	4.10E-01
	0.50	2.4247	4.98E-01
	0.75	47.2347	3.04E-01
Low	0.25	-159.9493	3.78E-02
	0.50	-122.9474	8.59E-02
	0.75	-45.5421	2.82E-01

Table S3 | Integrated water vapour transport (IVT, $kg\,m^{-1}\,s^{-1}$).

Group	Quantile	Obs. Diff.	p-value
Fully	0.25	387.0842	3.00E-04
	0.50	370.9310	1.40E-03
	0.75	375.2785	8.10E-03
High	0.25	263.5821	1.19E-01
	0.50	407.6834	4.35E-02
	0.75	192.2832	1.95E-01
Medium	0.25	230.7846	8.76E-02
	0.50	306.4890	1.48E-02
	0.75	483.2622	1.61E-02
Low	0.25	12.0756	3.75E-01
	0.50	1215.0571	6.50E-03
	0.75	1277.0715	2.82E-02

Table S4 | Moisture uptake from atmospheric river (AR)-efficient flux (%).

Group	Quantile	Obs. Diff.	p-value
Fully	0.25	-1.7804	1.50E-01
	0.50	-3.5170	6.00E-02
	0.75	-3.2718	9.00E-02
High	0.25	-0.7819	2.80E-01
	0.50	-0.8083	4.40E-01
	0.75	1.1156	4.40E-01
Medium	0.25	-5.4853	2.00E-02
	0.50	-1.6751	2.09E-01
	0.75	-1.3420	3.39E-01
Low	0.25	-4.2127	2.65E-01
	0.50	4.2993	2.43E-01
	0.75	22.3394	5.78E-02

Table S5 | Total moisture uptake (m).

Group	Quantile	Obs. Diff.	p-value
Fully	0.25	41.3336	2.75E-02
	0.50	24.9113	1.11E-01
	0.75	37.5328	1.80E-01
High	0.25	-0.4157	5.06E-01
	0.50	-35.4045	1.61E-01
	0.75	-25.9417	3.88E-01
Medium	0.25	70.7785	1.10E-01
	0.50	41.9318	4.89E-02
	0.75	134.0526	1.78E-02
Low	0.25	-89.4543	5.82E-02
	0.50	-134.2987	2.54E-02
	0.75	-118.6034	1.32E-01

Table S6 | Mean distance between the ETC centre and the AR axis (km).

Group	Quantile	Obs. Diff.	p-value
Fully	0.25	-1.32	3.97E-01
	0.50	4.41	3.35E-01
	0.75	39.45	9.50E-03
High	0.25	-18.98	2.39E-01
	0.50	0.83	5.07E-01
	0.75	-4.47	6.11E-01
Medium	0.25	9.08	2.98E-01
	0.50	28.59	2.63E-01
	0.75	-5.49	4.29E-01
Low	0.25	-79.51	1.91E-01
	0.50	10.37	5.06E-01
	0.75	-24.49	4.42E-01

Quantile permutation test results comparing fully associated and low-associated extratropical cyclones (ETCs) across historical and future periods. One-tailed p values < 0.05 are shaded.

Table S7 | Central mean sea level pressure (MSLP, hPa) of the ETCs.

Type	Quantile	Observed Difference	p-value
Hist.	0.25	-12.8	9.70E-03
E.C	0.25	-3.11	5.12E-01
Hist.	0.50	-13.4	2.80E-03
E.C	0.50	-5.03	4.13E-01
Hist.	0.75	-7.48	1.61E-02
E.C	0.75	-3.20	3.62E-01

Table S8 | ETC radius (km).

Type	Quantile	Observed Difference	p-value
Hist.	0.25	-82.4	2.46E-01
E.C	0.25	94.9	3.19E-02
Hist.	0.50	-39.3	6.20E-01
E.C	0.50	95.1	6.11E-02
Hist.	0.75	24.5	7.07E-01
E.C	0.75	120.0	1.35E-01

Table S9 | Integrated water vapour transport (IVT,$kg\,m^{-1}\,s^{-1}$).

Type	Quantile	Observed Difference	p-value
Hist.	0.25	877.0	1.60E-03
E.C	0.25	1250.0	4.00E-04
Hist.	0.50	1260.0	2.00E-04
E.C	0.50	411.0	4.61E-02
Hist.	0.75	1530.0	9.00E-04
E.C	0.75	627.0	4.98E-02

Table S10 | Total moisture uptake (m).

Type	Quantile	Observed Difference	p-value
Hist.	0.25	-82.0	7.19E-02
E.C	0.25	48.8	8.98E-02
Hist.	0.50	-77.2	1.20E-01
E.C	0.50	82.0	2.53E-02
Hist.	0.75	-80.7	2.89E-01
E.C	0.75	75.5	3.93E-01

Table S11 | Moisture uptake from atmospheric river (AR)-efficient flux (%).

Type	Quantile	Observed Difference	p-value
Hist.	0.25	35.9	0.00E+00
E.C	0.25	38.3	1.00E-04
Hist.	0.50	42.6	0.00E+00
E.C	0.50	34.8	1.00E-04
Hist.	0.75	46.6	0.00E+00
E.C	0.75	20.9	1.00E-04

Table S12 | Mean distance between the ETC centre and the AR axis (km).

Type	Quantile	Observed Difference	p-value
Hist.	0.25	-84.3	2.80E-03
E.C	0.25	-6.11	7.67E-01
Hist.	0.50	-114.0	6.00E-04
E.C	0.50	-120.0	3.20E-03
Hist.	0.75	-140.0	1.80E-03
E.C	0.75	-76.1	1.24E-02

The 85th percentile to quantify the most intense ETCs

The delineation of the most intense systems can vary depending on the criteria employed, including minimum central mean sea level pressure (MSLP), wind speeds, impact-based metrics, or vorticity. In this study, we identify intense systems using the radial horizontal MSLP gradient, defined as

$$\text{Gradient} = \frac{\text{MSLP}_{\text{LCI}} - \text{MSLP}_{\text{central}}}{R}, \tag{1}$$

where $\text{MSLP}_{\text{central}}$ and MSLP_{LCI} denote the central and outermost closed isobar pressures, respectively, and R is the system's radius. We focus on cases exceeding the 85th percentile of the gradient distribution over the historical period (1985–2014), a choice supported by a thorough review of the data.

To evaluate the robustness of this threshold, we tested multiple percentile levels (85th, 90th, 95th, and 99th). The 85th percentile provided a balanced sample size across the North Atlantic Ocean and its subregions, allowing for a more nuanced analysis (Table S13).

Table S13 | Number of sampled cyclone cases in the Western, Northern, and Eastern North Atlantic (NATL) for each $\Delta p/R$ percentile threshold (99th, 95th, 90th, 85th). Values in parentheses indicate the percentage of cases in each region relative to the total number of systems selected for the corresponding threshold.

Percentile Threshold	Western NATL	Northern NATL	Eastern NATL
99th	15 (75%)	3 (15%)	2 (10%)
95th	58 (60%)	31 (32.29%)	7 (7.29%)
90th	99 (59.28%)	53 (31.74%)	15 (8.98%)
85th	128 (60.38%)	64 (30.19%)	20 (9.43%)

Although the 85th percentile may be regarded as a conservative threshold for identifying extreme values of the $\Delta p/R$ gradient, its performance remains robust. To assess the sensitivity of the selection to this choice, we examined the joint distribution of the two components of the ratio—pressure depth (Δp) and radius (R)—for all cases retained under the different percentile criteria. Figure S4 presents the distributions of both parameters across cases, grouped by $\Delta p/R$ percentile.

Overall, increasing the percentile threshold preferentially selects systems with relatively small radii (i.e., a reduced denominator) or, alternatively, systems with sufficiently large pressure depths to compensate for larger radii. Conversely, relaxing the threshold from the 95th to the 85th percentile (Fig. S4 a–c) admits a greater number of storms with larger radii and pressure depths in the 25–45 hPa range. These depth values are nevertheless consistent with those typically exhibited by intense ETCs over the Atlantic basin, as reported in reanalysis-based studies (Papritz et al., 2021; Coll Hidalgo et al., 2025).

Importantly, when referenced against the interquartile range of Δp for the complete storm-track dataset, even the depths included under the 85th-percentile criterion exceed the 85th percentile of the full Δp distribution. Although larger systems reduce the gradient magnitude, the radii of the selected storms remain between the 25th and 75th percentiles—and never exceed the 85th percentile—of the overall radius distribution. This ensures that the $\Delta p/R$ metric is not disproportionately influenced by anomalously large or anomalously small systems.

Finally, we tested whether the central pressure characteristics of the selected storms are sensitive to the percentile choice. The proportion of cases falling within the lowest quartile of central MSLP varies only marginally across thresholds: 85%, 88.6%, 88.5%, and 90% for the 85th, 90th, 95th, and 99.9th percentiles, respectively. This consistency indicates that the identification of intense systems is stable with respect to the threshold choice, and that the 85th percentile remains a conservative and defensible criterion.

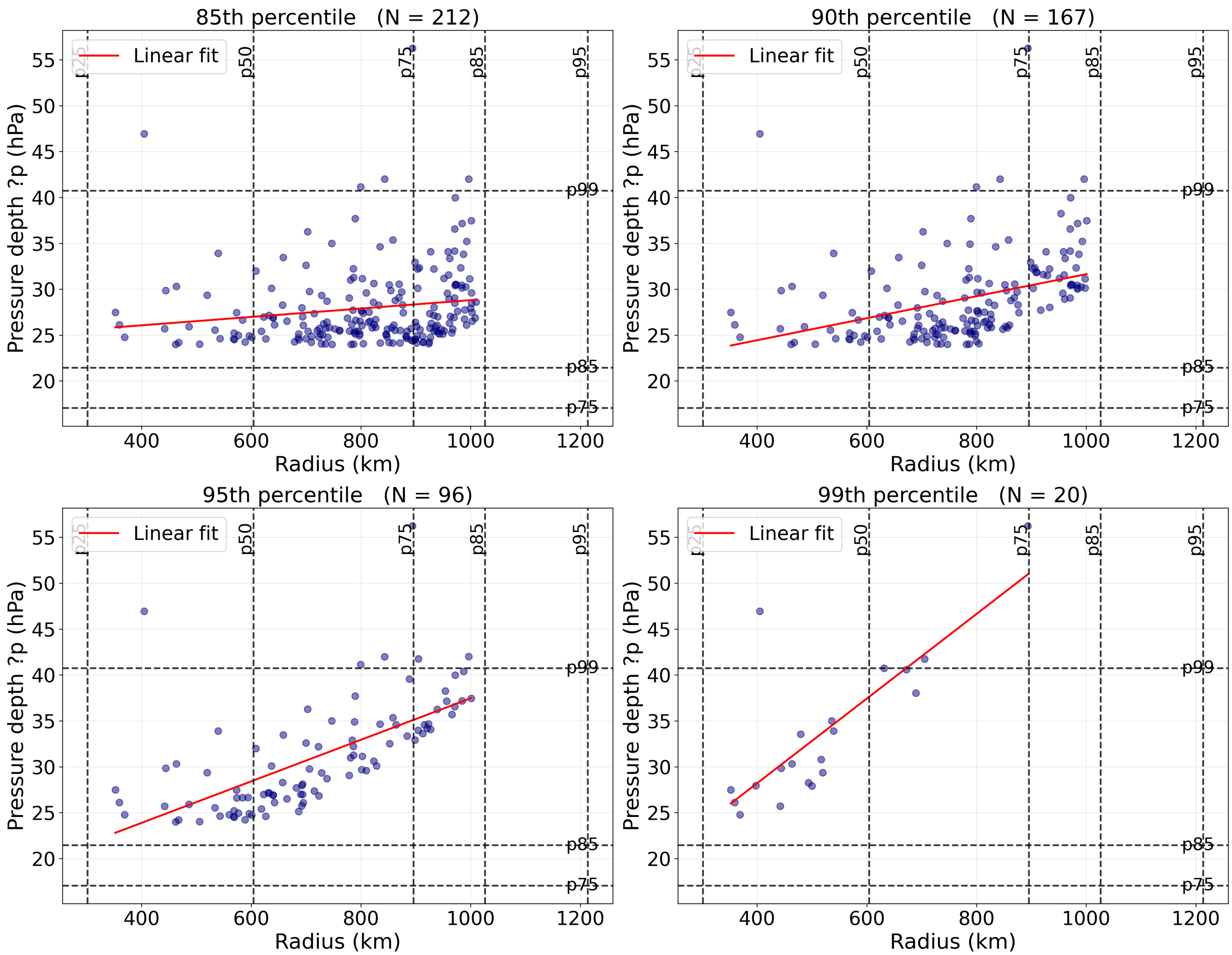

Figure S4 | Relationship between cyclone radius and pressure depth across $\Delta p/R$ percentile-selected cases. (a–d) Distribution of radius versus pressure depth ($\Delta p = \mathrm{MSLP_{LCI}} - \mathrm{MSLP_{center}}$) for cyclone cases selected above the 85th, 90th, 95th, and 99th percentiles of $\Delta p/R$, respectively. Dashed lines mark the percentiles of the pressure-depth (horizontal) and radius (vertical) distributions for the full half-year winter storm-track dataset for the historical period (1985–2014).

The ETC-AR coupling rate

The linkage between ETCs and ARs was evaluated by quantifying the contribution of AR-associated moisture fluxes to precipitation within the ETC radius. For each ETC at every time step, backward Lagrangian trajectories were computed to identify the sources of precipitating moisture over the preceding 10 days. The AR coupling analysis focused specifically on the final 24 hours, as the majority of moisture uptake events contributing to precipitation near ETC centers occur shortly before the precipitation event (Papritz et al., 2021). The degree of association between ETCs and ARs was then quantified as the ratio of life steps during which coupling occurred to the total ETC lifespan. Thresholds for the degree of association were defined based on the percentiles of the distribution of these ratios over the historical climate period (1985–2014).

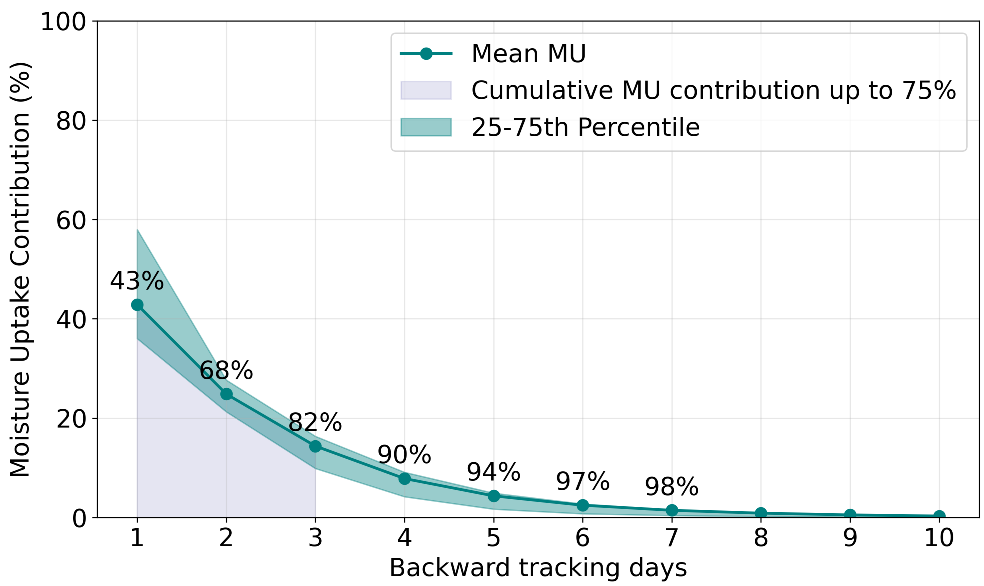

Figure S5 | Distribution and cumulative buildup of moisture uptake along 10-day backward trajectories. Mean daily moisture-uptake (MU) contributions across all trajectories ($N = 212$), with the interquartile range (25–75%; shaded). Labels indicate the cumulative fraction of total MU achieved by each backward-tracking day. The light-purple shading marks the period during which more than 75% of the total 10-day MU is accumulated.

To assess the sensitivity of ETC–AR coupling to the choice of moisture source period (i.e., the timeframe over which moisture gains are considered prior to precipitation), we first analyzed the daily contribution of moisture uptake relative to the total moisture contributing to ETC-related precipitation. Figure S5 shows both the distribution of mean daily percentages and their cumulative sum. The analysis reveals that, three days before precipitation, more than 75% of the moisture that contributes to the precipitation of the ETC had already been acquired. While using a 24-hour period to integrate specific humidity gains and delineate source regions strengthens the direct relevance of the coupling and reduces ambiguity in attributing contributions from ARs, we further explored the implications for classifying the degree of association by considering moisture sources from 24-, 48-, and 72-hour backtracking periods of precipitating air parcels.

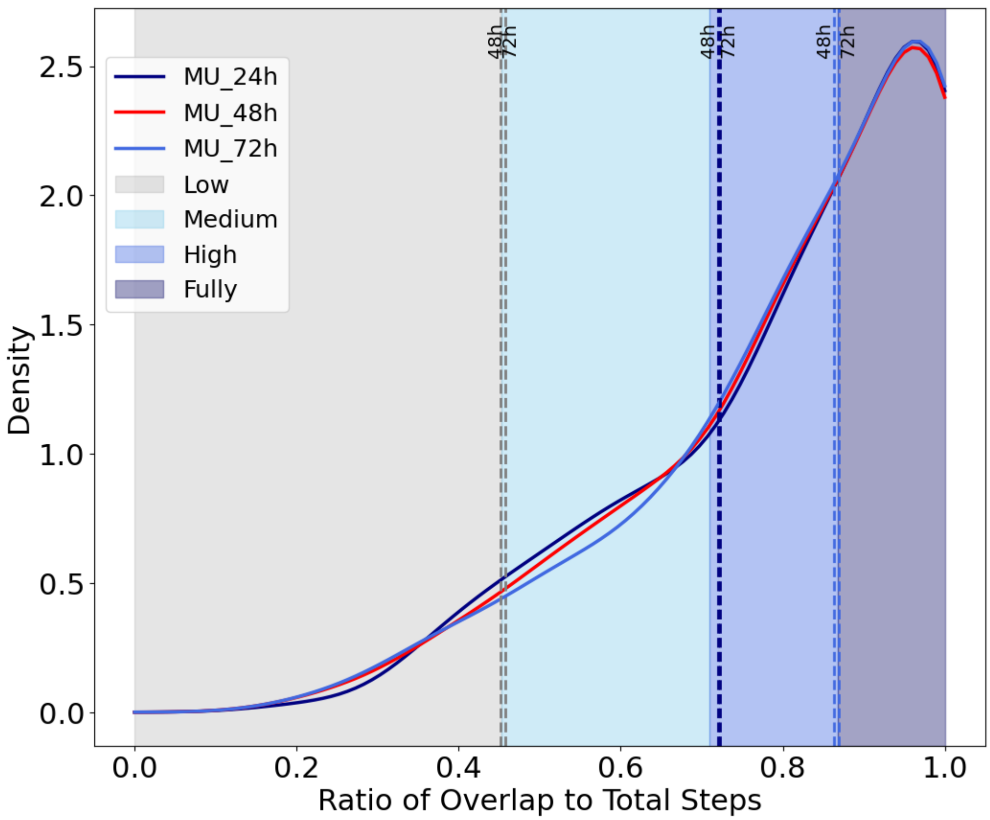

Figure S6 | Association between intense North Atlantic extratropical cyclones (ETCs) and atmospheric rivers (ARs) during the historical climate period (1985–2014). The distribution of the ratio of ETC life steps associated with ARs to the total ETC lifespan is shown. A coupling between ETCs and ARs is recorded when the ETCs' moisture uptake region within a time period spatially overlaps an AR footprint. Distributions are shown for moisture sources based on specific humidity gains over the 24, 48, and 72 hours preceding precipitation. Shaded bands indicate thresholds of low (L), medium (M), high (H), and full (F) coupling for 24-hour MUs, while dotted lines represent corresponding thresholds for longer-duration MU periods.

Figure S6 displays the distributions of the overlap ratio between ETC moisture sources and ARs for cases in the historical period. The 25th, 50th, and 75th percentiles of these distributions were used to define the degree of association: cases below the 25th percentile were classified as weakly coupled (Low), those between the 25th and 50th percentiles as moderately coupled (Medium), those between the 50th and 75th percentiles as strongly coupled (High), and those above the 75th percentile as fully or nearly fully associated with ARs throughout their lifetime.

Varying the definition of moisture sources according to the period used to calculate moisture gains prior to precipitation resulted in highly consistent distributions across the 24-, 48-, and 72-hour periods, with percentile thresholds remaining largely unchanged. Regarding the impact on case classification, using the 48- and 72-hour periods led to minimal differences compared to the 24-hour criterion. For the 48-hour period, fully associated cases increased by one at the expense of strongly associated cases, while for the 72-hour period, strongly associated cases increased by one, drawn from the moderately associated category. These results demonstrate that the degree of ETC–AR association is robust to the choice of moisture source period.

References

Papritz, L., Aemisegger, F., & Wernli, H. (2021). Sources and transport pathways of precipitating waters in cold-season deep North Atlantic cyclones. *Journal of the Atmospheric Sciences*, *78*(11), 3349–3368. https://doi.org/10.1175/JAS-D-21-0105.1

Coll-Hidalgo, P., Nieto, R., Fernández-Alvarez, J. C., & Gimeno, L. (2025). Assessment of the origin of moisture for the precipitation of North Atlantic extratropical cyclones: Insights from downscaled ERA5. *Atmospheric Research*, 108205. https://doi.org/10.1016/j.atmosres.2025.108205